March 20, 2017

A new experimental approach to probe QCD Axion Dark Matter in the mass range above 40 μeV

The MADMAX interest group:
P. Brun,[a] A. Caldwell,[b] L. Chevalier,[a] G. Dvali,[b,c] E. Garutti,[d] C. Gooch,[b] A. Hambarzumjan,[b] S. Knirck,[b] M. Kramer,[e] H. Krüger,[f] T. Lasserre,[a] A. Lindner,[f] B. Majorovits [b,1] C. Martens,[f] A. Millar,[b] G. Raffelt,[b] J. Redondo [g,2] O. Reimann,[b] A. Schmidt,[d] F. Simon,[b] F. Steffen,[b] G. Wieching[e]

[a]CEA-IRFU, Saclay, France
[b]Max-Planck-Institut für Physik, Munich, Germany
[c]LMU, Munich, Germany
[d]University of Hamburg, Hamburg, Germany
[e]Max-Planck-Institut für Radioastronomie, Bonn, Germany
[f]DESY, Hamburg, Germany
[g]University of Zaragoza, Spain

Abstract. Axions represent a class of particles that emerge in theoretical models explaining several mysteries of high-energy particle physics and cosmology. They explain the absence of CP violation in the strong interaction, provide dark matter candidates, and can be responsible for inflation and structure formation in the early universe. Several searches for axions and axion-like particles have constrained the parameter space over the last decades, however, no hints of axions have been found. The mass range of 1–1000 μeV remains highly attractive and well motivated region for dark matter axions. In this White Paper we present a description of a new experiment based on the concept of a dielectric haloscope for the search for dark matter axions in the mass range 40–400 μeV. The experiment, called MADMAX, will consist of several parallel dielectric layers, whose separations can be adjusted and are placed in a strong magnetic field. This would lead to the emission of axion induced electromagnetic waves in the 10–100 GHz domain, with the frequency given by the axion mass.

[1]Corresponding author, Email: bela.majorovits@mpp.mpg.de,
[2]Corresponding author, Email: jredondo@unizar.es

Contents

1 Introduction

Axions are hypothetical low-mass bosons predicted by the Peccei-Quinn (PQ) mechanism, which explains the absence of CP-violating effects in quantum chromodynamics (QCD). Axions could also provide the cold dark matter of the universe and as such are among the few particle candidates that simultaneously resolve two major problems in physics.

Assuming axions make up all the dark matter in the universe, whose mass is expected to be between 1–1000 μeV. Lower masses are thought to be unnatural, as this would require the initial misalignment angle to be unnaturally small, negating the original motivation for introducing it. Masses higher than 10 meV are excluded due to astrophysical constraints [1]. The existing experimental efforts for dark matter axion searches focus on a range of axion masses below $\sim 40\,\mu$eV which is motivated by the traditional re-alignment mechanism of the axion field. Microwave cavity searches, notably from ADMX [2] and ADMX-HF [3], have recently begun to probe part of this parameter space.

If the PQ symmetry was restored after inflation, decaying topological defects could lead to an axion population providing all of the cold dark matter with an axion mass of the order 100 μeV [4–9].

We propose to search for QCD axion dark matter in the mass range around 100 μeV, using a dielectric haloscope [10], making use of the "dish antenna" idea [11] in combination with broad-band resonant effects expected by dielectric layers [12].

This White Paper discusses the principles upon which dielectric haloscopes are based. A first baseline design that could be used for the search of axions with mass 40–400 μeV is described as well as the results of the investigations that have been preformed to date. These lead us to the conclusion that it should be realistic to build a setup that can cover a large fraction of the parameter space predicted for dark matter axions in the post inflationary Peccei-Quinn symmetry breaking scenario.

2 Theoretical motivation

2.1 Strong CP problem

In the the standard model (SM) of particle physics, violation of CP in the strong interactions is controlled by just one parameter, the θ angle. This angle appears as the sum of two contributions with a-priori unrelated origins: the angle defining the vacuum of quantum-chromodynamics (QCD), θ_{QCD}, and the common phase of the quark mass matrix, $\mathrm{Arg\,Det}\, M_q$, related to the Yukawa couplings of the Higgs sector. When we redefine quark fields to make their masses real, the phase appears as the coupling constant of the topological charge density operator of QCD, i.e. the SM Lagrangian contains a term

$$\frac{\alpha_s}{8\pi}\widetilde{G}_a^{\mu\nu}G_{\mu\nu a}\theta, \tag{2.1}$$

which violates parity, time-reversal and thus CP. Nonzero values of θ imply CP violating observables such as nuclear electric dipole moments but none of these effects have been observed to date. As a key example, the electric dipole of the neutron is predicted to be $d_n = 4.5 \times 10^{-15}\,\theta$ e cm [13] but the most recent experiment [14] concluded that $d_n < 2.9 \times 10^{-26}$ e cm, so θ must

be extremely tiny, $\theta < 6.4 \times 10^{-12}$. This is an amazingly small upper limit, especially if we consider that the only other CP violating phase in the SM, the CKM angle $\delta_{13} = 1.2 \pm 0.08$, is not particularly small and also comes from the quark mass matrix. Technically, this is not a problem in the SM because θ runs very slowly with the renormalisation scale, but in extensions of the SM with additional CP violation, such as supersymmetry, the implied small shift from zero can be a serious issue. In any case, the smallness of CP violation gives us a hint that some dynamical mechanism could be at work to suppress the effects of θ.

2.2 Axions

In 1977 Peccei and Quinn proposed a mechanism to solve the strong CP problem, often considered to be the most elegant to date [15, 16]. They realized that the vacuum energy density of QCD depends on θ, i.e. $V_{\rm QCD} = V_{\rm QCD}(\theta)$, and its absolute minimum lies[1] at $\theta = 0$ [18], which is CP conserving! If θ is interprited to be a dynamical field, $V_{\rm QCD}(\theta)$ becomes the potential energy of that field so the expectation value $\langle\theta\rangle$ will be dynamically driven to zero, explaining the absence of CP violation.

This mechanism has three model-independent consequences which are of relevance to us:

- Excitations of $\theta(x)$, where x is position, around the minimum of the potential represent a new particle, the axion.

- The dynamical $\theta(x)$ field needs a kinetic term $f_a^2(\partial_\mu\theta)(\partial^\mu\theta)/2$, which requires a new energy scale f_a. The axion field is the canonically normalized version of θ, $a(x) = \theta(x) f_a$. Values $f_a \lesssim 10^8$ GeV are excluded experimentally and astrophysically, so the axion offers a window to discover physics at ultra-high energies not testable by current accelerator techniques.

- The cancelation of $\langle\theta\rangle$ is dynamical, leading to residual oscillations of θ around the minimum, which are expected for generic initial conditions. As the life-time of the Universe finite, these oscillations are particles that could constitute today's cold dark matter.

The θ angle has the same quantum numbers as the $\eta_8 \sim \bar{u}u + \bar{d}d + \bar{s}s$ quark bilinear. Thus, the axion mixes with η_8 and through η_8 with π_0. This mixing leads the axion to acquire the properties of these mesons, although with values suppressed by a small mixing angle $\sim f_\pi/f_a$. For our purposes, the most relevant properties are the axion mass

$$m_a = 5.70(6)(4)\,\mu\text{eV}\left(\frac{10^{12}\,\text{GeV}}{f_a}\right), \tag{2.2}$$

and the interaction with two photons

$$\mathcal{L}_{a\gamma\gamma} = \frac{\alpha}{2\pi} C_{a\gamma} \frac{a}{f_a} \mathbf{E}\cdot\mathbf{B} \qquad \text{with} \qquad C_{a\gamma} = 1.92(4) - \frac{\mathcal{E}}{\mathcal{N}}, \tag{2.3}$$

both recently computed at NLO in χ perturbation theory [19]. Numbers in brackets denote the uncertainty in the last digit of the axion mass, with the referring to the uncertainty in the up-down quark mass ratio and the second comes from higher order effects. In the coupling to two photons, $C_{a\gamma}$, the numerical factor 1.92(4) comes from meson mixing and the factor $\mathcal{E}/\mathcal{N}$ is the model-dependent radio of the electromagnetic and colour anomalies.

[1] Strictly speaking, this would only happen if $\delta_{13} = 0$ but CP violation is transmitted by quantum corrections to the QCD sector and the minimum gets shifted from $\theta = 0$ by a small amount. See [17] for a review.

One popular way of realizing the PQ mechanism is to add extra quarks to the SM and give them mass through additional Higgs-like particles which take a vacuum-expectation-value (VEV) of the order of $\sim f_a$. The axion field is the pseudo-Nambu-Goldstone boson associated to the diagonal axial symmetry which is spontaneously-broken when the new quarks acquire mass, i.e. the equivalent of η_8 of the new quarks. This symmetry is color anomalous (necessary ingredient for the NGB to become the axion), but can also have an electromagnetic anomaly of its own if the new quarks are charged.

The most important model dependency for our purposes is the so-called domain-wall number $\mathcal{N}$. When building axion models we often end up defining the axion field as $a/f_a = \mathcal{N}\theta$ with $\mathcal{N}$ an integer, not necessarily 1. In other words, one can write down models in which the axion field can wrap up more than once around the same QCD potential. In other words, $\theta = 0$ and $\theta = 2\pi$ would correspond to two physically different values of the axion field, even if from the QCD potential perspective they would be identical. In these models there are $\mathcal{N}$ physically equivalent vacua that solve the strong CP problem and domain wall axion field configurations that interpolate between them.

2.3 Models

The original model of PQ related f_a to the electroweak scale, using the SM Higgs and fermions. As these axions interacted relatively strongly, with f_a being given by the electroweak scale, they were quickly excluded. Generic axion models with much larger f_a were soon proposed and dubbed "invisible" for their feeble interactions. These are the archetypal KSVZ [20, 21], DFSZ [22, 23], and variant axion models [24, 25]. The main detectable effect for our purposes is that $\mathcal{E}$ and $\mathcal{N}$ depend on the specific model; the KSVZ and DFSZ models often serve as benchmarks with $\mathcal{E}/\mathcal{N} = 0$ and 8/3, respectively.[2] However, it is important to note that not all axion models have $C_{a\gamma} = \mathcal{O}(1)$ [26]. In [26] the authors considered couplings to photons which could be significantly enhanced with $\mathcal{E}/\mathcal{N} = 170/3 \sim 57$, or substantially reduced if $\mathcal{E}/\mathcal{N} = 23/12 \sim 1.92$. In the scenario which we will consider, models with $\mathcal{N} = 1$ are preferred by cosmology, as discussed in section 3.

While one considers axion models without making assumptions about the solutions of other cosmological problems, they generally fit very nicely into extensions of the standard model, often resolving multiple issues at once. For example, the SMASH models [27] simultaneously resolve the strong CP problem, dark matter, baryogenesis, inflation and neutrino masses. The PQ mechanism can also be very efficiently embedded in supersymmetric extensions of the SM [28–30]. In this context, not only can one resolve the strong CP problem, as well as DM, but DFSZ axions can resolve the μ problem of supersymmetry via the Giudice-Masiero mechanism [31]. The μ problem is the requirement that the supersymmetric Higgs mass term μ must be of the scale of soft supersymmetry breaking, rather than close to the Planck mass as one would naively expect. In addition, axions and the similar axion-like particles (ALPs) are natural predictions of string theory [32]. As discussed below not only one but many axion candidates can arise in the process of compactification [33] although there is no guarantee that they remain light.

2.4 Axion-like particle (ALPs) and weakly interacting slim particles (WISPs)

As mentioned above, the QCD axion fits nicely in embeddings of the standard model. In field theoretic models it can be invoked as a pseudo-Nambu-Goldstone (pNGB) boson and it appears

[2] However, it is straightforward to generalize KSVZ to have different $\mathcal{E} \neq 0$ and there are two known variants of DFSZ with $\mathcal{E}/\mathcal{N} = 2/3$ and 8/3 respectively.

naturally in string models. Actually, both types of particles pNGBs or stringy "axions" are generically expected from field theory models and stringy models. In field theoretic extensions of the SM we expect more fields and more symmetries as we consider particle physics at higher and higher scales so pNGBs are a natural possibility. In string theories, there are typically hundreds of moduli with their consequent axion-like-particles, see [34] for a review. Whether these particles get a small mass or not, or if they couple to QCD to become the QCD axion, depends very strongly on the details of the model. A priori one can expect that besides the QCD axion many axion-like particles (ALPs) can exist. The low energy effective Lagrangian of an ALP associated to a high-energy scale f_ϕ is essentially the same as that of the axion, however without as rigid a relationship. An ALP can have a coupling to photons, quarks (or baryons), leptons, etc. If the ALP couples to the $\widetilde{G}G$ operator or appears in quark Yukawa interactions it can become the QCD axion. In case of many ALP candidates, only one linear combination becomes the true QCD axion and orthogonal combinations can still couple to photons, baryons, etc., but their masses will be completely unrelated to that of the QCD axion, which is given by (2.2). These particles can have a very similar phenomenology to the QCD axion. In particular they can be the cold dark matter of the Universe [35], and as such could be detected by many of the experiments searching for the QCD axion. Indeed, most of the QCD axion experiments are ALP experiments; they would have a hard time differentiating between the QCD axion and an ALP in the event of a discovery. From a practical point of view, this justifies paying attention to a larger range of parameter space in the axion-mass and two-photon coupling plane. Although axions are naively expected to be relatively near the KSVZ or DFSZ lines, ALPs could exist with much smaller or larger photon couplings for a given mass.

The phenomenology of these ALPs is less constrained than that of QCD axions, which allows one to explain some puzzling phenomena with ALPs with judiciously chosen couplings and mass. For instance, the anomalous transparency of the Universe to very high energy gamma rays could be explained with an ALP of very small mass $m_\phi \sim$ neV but a sizeable coupling to photons $g_{\phi\gamma\gamma} \sim 10^{-11}$ GeV^{-1}, see [36] for a recent review with further references. In addition, as discussed below some anomalies in the cooling of stellar objects could also be explained by ALPs.

The phenomenology of axions and ALPs is to some extent parallel to other weakly interacting low mass bosons. A notable example is given by "hidden photons" (HP) (also called paraphotons, dark photons, ...), gauge bosons of a U(1) symmetry under which SM particles have no charge. These HPs can mix with photons in vacuum through kinetic mixing giving many of the effects sought for axion-photon mixing in an external B-field, with the drawback that photon-HP mixing effects will happen without B-field. Most notably, these effects include the axion DM conversion into photons described in this project. So we shall keep an open mind when analyzing data of any axion experiment, as it can have consequences for other "less expected" weakly interacting slim particle (WISP). Therefore even without a magnet our approach gives us the possibility to detect well motivated DM candidates. Reviews on WISPs, axions and the synergies in their experimental search can be found in [37, 38].

2.5 Landscape

Our experimental knowledge on f_a—equivalently m_a—is model-dependent to the extent that the observable effects on axions depend on its couplings, which have model-dependent contributions. Thus one either quotes constraints on a specific coupling, e.g. $C_{a\gamma}$ as a function of m_a, or one needs to specify a particular model. Note that for ALPs do not have the tight mass relation given by (2.2), but $C_{a\gamma}$ can still be defined as in (2.3). However, for a broad first picture of

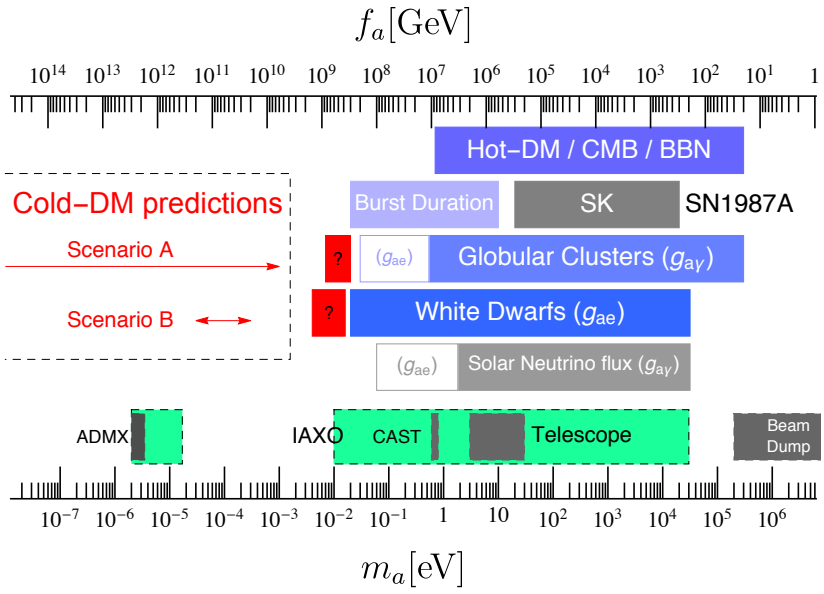

Figure 1. Overview of axion mass bands (equivalently f_a) excluded by a variety of astrophysical and cosmological arguments (blue) or laboratory searches (gray) together with experimental prospects (green) and axion cold dark matter predictions. Scenarios A and B are defined in section 3

the arguments that have been used to exclude axions we can simply assume that all the axion couplings are order one. This is shown in Fig. 1 as a function of f_a, which sets the axion mass and the base strength of the axion couplings. A combination of stellar evolution and cosmological arguments together with experimental searches rule out axions with $f_a < 10^8$ GeV, $m_a > 30$ meV. Most of the invisible axion parameter range is excluded by the impact that axion emission would have in different stellar objects: SN1987A, horizontal-branch and red giant stars in globular clusters, white dwarves and the Sun (see [1] for a summary). Generally speaking, as axions interact weakly they would serve as a mechanism for energy loss. By not observing this energy loss we gain an upper bound on the interaction strengths (and masses, depending on the kinematics).

Close to the axion mass limit, $m_a \sim 10$ meV, axion emission and the inherent exotic stellar energy loss channel typically have $O(1)$ effects on stellar observables. Interestingly, some of the observed systems; white dwarves, horizontal branch stars in globular clusters and the tip of the red giant branch of the globular cluster M5, show a slight preference for exotic cooling and could be hinting at an axion or ALP with $f_a \sim 10^9$ GeV [39].

Since the axion coupling to photons is crucial for this proposal it is interesting to review the experimental limits on any axion-like particle coupled to photons in the $C_{a\gamma} - m_a$ plane. Unlike a QCD axion, for a generic ALP the relation between its decay constant f_a and its mass is not fixed. Thus it proves convenient to define a generic ALP-photon coupling from the interaction term:

$$\mathcal{L} \in g_{a\gamma\gamma}\, a\, \mathbf{E} \cdot \mathbf{B}. \tag{2.4}$$

Constraints on a general ALP are compiled in Fig. 2.

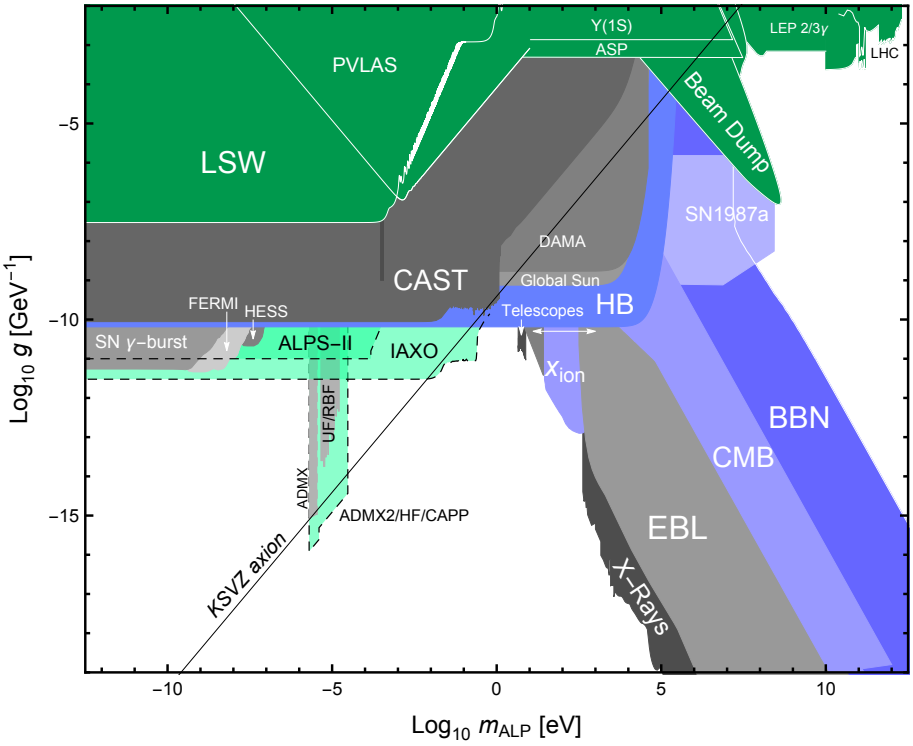

Figure 2. Constraints on a generic ALP with mass and coupling to two photons. Also shown the prospects for the reach of IAXO, ALPS-II and axion dark matter experiments ADMX, ADMX-HF and CAPP.

2.6 Axion dark matter

Dark matter axions can be produced in the early universe by at least two processes: in reactions from SM particles in the thermal bath (thermal axions) and by the vacuum realignment mechanism (non-thermal axions). The thermal population is created with momenta similar to the temperature of the Universe, while the non-thermal population has much smaller momenta, on the order of the causal Horizon. Thermal axions constitute hot dark matter like ordinary neutrinos, while realignment axions constitute cold dark matter. Axions that satisfy the astrophysical constraints are so weakly-interacting and have such small masses that the cold, non-thermal, population strongly dominates.

In the vacuum realignment mechanism, the axion field starts with certain initial conditions, which then evolve as driven by its potential energy, $V_{\rm QCD}$. The axion dark matter yield is thus determined by initial conditions and not by thermodynamics.

Broadly speaking we can consider two types of axion cosmologies. They differ in the order of two critical events: cosmic inflation and the PQ phase transition. The axion is an angular field defined $a \in (-\pi, \pi) f_a$. Note that the low energy description we use is expected to break down at energy scales $\sim f_a$: at energy scales higher than f_a other degrees of freedom will be relevant. The PQ phase transition is the moment in the early Universe when these unknown elements recombined or are restructured, leaving the axion field (and possibly others) as propagating degrees of freedom. For an analogy, recall that quarks and gluons are the relevant degrees of freedom of high energy QCD, but when the temperature of the Universe decreased below $\Lambda \sim 150$ MeV, the strong force became confining, combining them into baryons and mesons. The PQ phase transition happens at energy scales $\sim f_a \gg \Lambda$, where the strong interactions

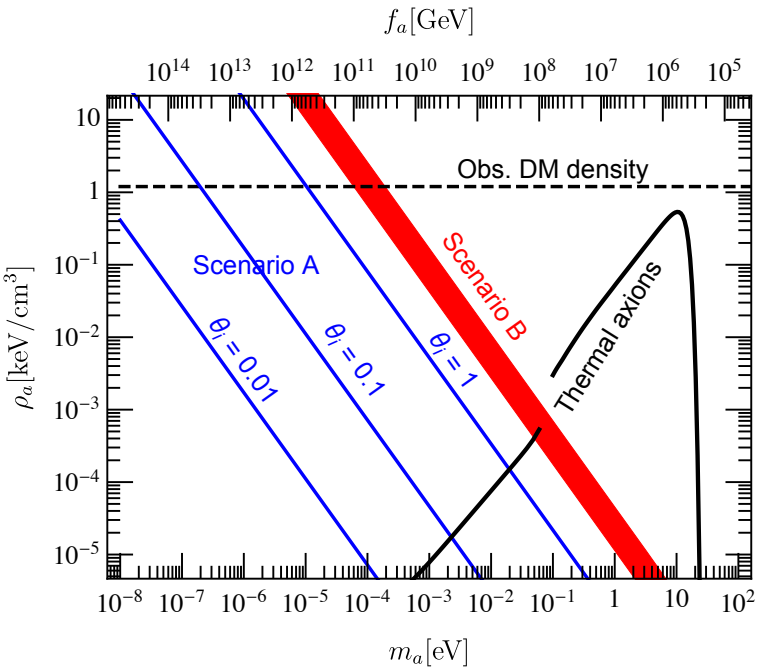

Figure 3. Axion dark matter density today as a function of mass for several values of θ_i in Scenario A and Scenario B ($N_{\rm DW} = 1$) according to [4, 5]. Also shown the thermal component relevant at high masses.

are perturbative and $V_{\rm QCD}$ is extremely suppressed. This has the interesting consequence that when axions are "born" they have effectively no potential, so no value of $\theta \in (-\pi, \pi)$ is preferred. As a consequence, after the PQ phase transition different causally disconnected patches of the Universe will have different values of what we call the initial misalignment angle θ_i. Let us consider now the two cosmologies.

In Scenario A, inflation happens *after* the PQ phase transition. A small patch within the horizon, small enough that it is homogeneous in θ_i, increases in size exponentially to become larger than our observable Universe. The initial value of the axion field in our local Universe is unique—up to quantum fluctuations—and it is fundamentally unpredictable from first principles. In this scenario, one can have the complete amount of cold dark matter observed, i.e. $\Omega_c h^2 = 0.12$, in the form of cold axions for any value of $f_a \in (M_p, 10^9 {\rm GeV})$, assuming a suitable value of the initial universal misalignment angle $\theta_i(f_a)$, see [8]. Several examples are plotted as blue lines in Fig. 3.

In Scenario B, inflation happens *before* the PQ phase transition. The axion field remains a patchy structure from the PQ phase transition until today. From the PQ phase transition until QCD confinement the axion field is massless and thus its correlation length increases with the causal horizon. When $V_{\rm QCD}$ becomes relevant, the axion field becomes massive and starts to move towards $\theta = 0$, eventually oscillating around it. Here, the co-moving size of inhomogeneities stops increasing as axions are non-relativistic and so cannot free-stream. Thus our local Universe today contains many patches where the initial conditions of the axion field were essentially random. Because of this, one can perform an statistical average to obtain a prediction $\Omega_c h^2 = \Omega_c h^2(f_a)$.

Scenario B is complicated by the presence of cosmic strings. After the PQ phase transition, a network of global cosmic strings is formed with the axion field. Cosmic strings are locations

where the order parameter of the PQ phase transition is topologically constrained to be in the symmetric high/energy phase. Consider a circle where θ takes values from $-\pi$ to π. As we shrink the circle the θ values are bound to span $(-\pi, \pi)$ but the circle contracts to a single point, where the θ field cannot be multi-valued. At that point the PQ symmetry should be restored, leading to a small region with a high energy due to the axion field being far away from the minimum of the potential. Taking this analogy from 2 to 3D our point becomes a line. The existence of these axionic strings is intimately tied to the patchy axion initial conditions after the PQ phase transition. Small string loops contract and decay and long strings straighten and intersect to form small loops. In all these processes some energy converts into long-wavelength axions, which will also contribute as dark matter.

If $N_{\rm DW} = 1$, the network can disintegrate completely when the axion becomes massive, leaving only axions. For $N_{\rm DW} > 1$, the domain walls cannot pull the strings to a final end owing to the perfect degeneracy between the $N_{\rm DW}$ CP conserving vacua. A network of domain walls persists, which very soon dominates the energy density of the Universe, leading to a Universe completely at odds with observations. Thus the $N_{\rm DW} > 1$ case in Scenario B is only viable if a small breaking of the degeneracy between the vacua is included. But the situation is delicate as these breaking terms also affect the quality of the axion solution to the strong CP problem and may completely spoil it. An interesting possibility is that this breaking is induced by Planck suppressed operators, some of which are forbidden by discrete symmetries [41].

The calculation of axion string radiation is complicated due to the lack of a convincing analytical treatment and the huge dynamical range of the simulations required (the string thickness is $\sim 1/f_a$ while the causal Horizon at the moment of interest is $\sim 1/m_a$). The most recent attempt extracts the average axion energy radiated by strings and applies to it an axion energy density scaling solution [4, 5]. Assuming $N_{\rm DW} = 1$ this leads to the Scenario B prediction drawn as a red thick line in Fig. 3 (the errors have been slightly enlarged as discussed in [9]). The full amount of dark matter in axions is achieved in the mass range

$$50\ \mu\text{eV} \lesssim m_a \lesssim 200\ \mu\text{eV} \tag{2.5}$$

with $m_a \sim 100\ \mu$eV as the preferred value.

In $N_{\rm DW} > 1$ cases, the final axion density is significant so that the axion mass giving all the dark matter turns out to be much larger than when $N_{\rm DW} = 1$, see [4, 41]. Typically these masses are excluded by stellar evolution unless some fine-tuned parameters appear in the degeneracy breaking. With this tuning, axion dark matter in the 1–10 meV mass range is possible [40]. This high mass requires search techniques very different to the $100\,\mu$eV ballpark suggested by $N_{\rm DW} = 1$, so we will not consider them further.

Recent studies [42–44] propose the direct simulation of the axion yield. At the moment, they seem to indicate that less axion dark matter is generated for a given f_a. This would mean that m_a might be smaller than the $100\,\mu$eV figure. A first direct estimate suggested $20\,\mu$eV [42] but it was suggested that those simulations could be underestimating DM by a factor of 2, so 40μeV would be preferred. It seems too early to conclude with a sharp prediction, but several groups are working on this estimate. More precise predictions are to be expected in the next few years.

In any event, given the current bracketing figures, axions in Scenario B will require dedicated experimental efforts to be discovered, as so far no axion dark matter experiment had promising sensitivity above $\sim 20\,\mu$eV, as discussed below.

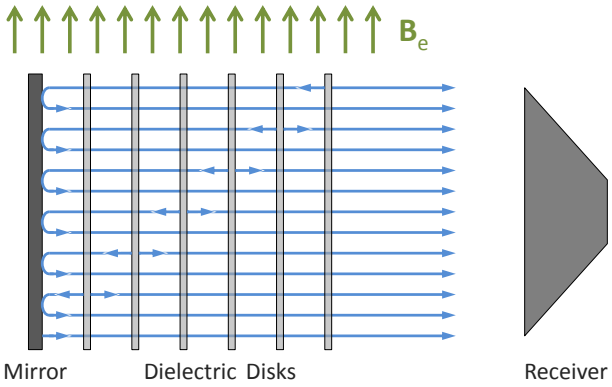

Figure 4. A dielectric haloscope consisting of a mirror and several dielectric discs placed in an external magnetic field $\mathbf{B}_e$ and a receiver in the field-free region. A parabolic mirror (not shown) could be used to concentrate the emitted power into the receiver. Internal reflections are not shown. Figure taken with permission from [10].

3 Foundations of experimental approach

With this understanding of cosmological axions, we can consider how one might look for such a particle. The most successful experiments to date are based on cavity resonators in strong magnetic fields (Sikivie's haloscopes [45]) such as ADMX [2], ADMX HF [3] or CULTASK [46]. However, these are optimal for $m_a \lesssim 20\,\mu$eV, which has been considered the most natural range for axion DM in Scenario A. For much lower values of m_a nuclear magnetic resonance techniques like CASPER [47] or with LC circuits [48, 49] could be effective. Unfortunately, the high mass regime has proven recalcitrant.

Because of this, the mass range favored in Scenario B is untouched by current experiments, and for cavity haloscopes will remain so for the foreseeable future. While fifth-force experiments [50] could search this region, they would not directly reveal the nature of dark matter. In [10] a new concept to cover this important gap was introduced, capable of discovering $\sim 100\,\mu$eV mass axions. It consists of a series of parallel dielectric discs with a mirror on one side, all within a magnetic field parallel to the surfaces as shown in Fig. 4—a dielectric haloscope. In this section we will follow the description contained in [10].

3.1 The principles of axion-photon conversion

As the axion interacts with photons via equation (2.3), it is worth seeing if one can use this interaction to produce a detectable signal. We are interested in galactic dark matter axions, which are in a highly occupied state and very non-relativistic ($v_a \lesssim 10^{-3}$). The associated de Broglie wavelength, $2\pi/m_a v_a \gtrsim 12.4\,\mathrm{m}\,(100\,\mu\mathrm{eV}/m_a)$, is larger than the dimensions of our dielectric haloscope, which will be roughly a cubic meter. Thus we treat θ as a classical field and take the zero-velocity limit, which implies an (approximately) homogeneous and monochromatic $\theta(t) \simeq \theta_0 \cos(m_a t)$.

The interaction (2.3) enters as a current on the right-hand side (RHS) of the Ampère-Maxwell equation,

$$\nabla \times \mathbf{B} - \epsilon \dot{\mathbf{E}} = \frac{\alpha}{2\pi} C_{a\gamma} \mathbf{B}\, \dot{\theta}, \tag{3.1}$$

for a medium with permeability $\mu = 1$ and dielectric constant ϵ. When a static and homogeneous

external magnetic field $\mathbf{B}_\mathrm{e}$ is applied, the axion dark matter field sources a tiny electric field

$$\mathbf{E}_a(t) = -\frac{\alpha}{2\pi\epsilon} C_{a\gamma} \mathbf{B}_\mathrm{e}\, \theta(t) \tag{3.2}$$

which is discontinuous at the interface between media of different ϵ. To satisfy the usual continuity requirements, $\mathbf{E}_{\parallel,1} = \mathbf{E}_{\parallel,2}$ and $\mathbf{B}_{\parallel,1} = \mathbf{B}_{\parallel,2}$ (recall $\mu = 1$), EM waves of frequency $\nu_a = m_a/2\pi$ must be present to compensate for the discontinuity. In other words, breaking translational invariance couples the approximately non-propagating axion-induced E-field with propagating EM waves, which we will aim to detect. The EM waves are emitted perpendicularly to the disc surfaces in our zero-velocity limit [11]. We require flat discs of large area to avoid diffraction, $A \gg \lambda_a^2$, so we can work in a 1D framework, as well as maximize the output power (which is proportional to A). To maximize the discontinuity in $\mathbf{E}_\parallel$, $\mathbf{E}_a \propto \mathbf{B}_\mathrm{e}$ must be parallel to the disc surfaces [11]. To allow us to extract a signal from the longitudinal direction, this will require us to use a dipole magnet.

The amplitude gain from a dielectric haloscope with respect to a mirror alone (a flat dish antenna [11]) can be quantified in terms of an amplitude boost factor β. Comparing the E-field inside the mirror ($E \simeq 0$) with the axion-induced one in vacuum $E_0 \equiv \alpha/(2\pi)\,|C_{a\gamma}\mathbf{B}_\mathrm{e}\,\theta_0|$, one finds that the continuity at the surface requires the emission of an EM wave of amplitude E_0 with a power per unit area $P_0/A = E_0^2/2$ [11]. With additional dielectric discs as shown in Fig. 4, the axion field induces plane EM waves for every change of media. By tuning the disc separations, constructive interference can enhance the amplitude of the emitted EM wave to E_out at the receiver. The amplitude boost factor is thus defined as

$$\beta(\nu_a) \equiv |E_\mathrm{out}(\nu_a)/E_0|. \tag{3.3}$$

With this definition, and E_0 as introduced above, the resulting output power of the dielectric haloscope per unit area is

$$\frac{P}{A} = \beta^2 \frac{P_0}{A} = 2.2 \times 10^{-27}\, \frac{\mathrm{W}}{\mathrm{m}^2}\, \beta^2 \left(\frac{B_\mathrm{e}}{10\ \mathrm{T}}\right)^2 C_{a\gamma}^2\,, \tag{3.4}$$

where β^2 is the power boost factor. The β is calculated by matching $\mathbf{E}_a$ in each region (dielectric disc or vacuum) with left and right-moving EM waves as imposed by the continuity of the total $\mathbf{E}_{||}$ and $\mathbf{B}_{||}$ fields at the interfaces. A transfer matrix formalism has been developed for this task, though one can also use generalized version of the more traditional overlap integral method [51].

The desired enhancement, $\beta \gg 1$, comes from two effects, which generally act together but can be differentiated in limiting cases. These effects depend on the optical thickness of one disc $\delta = 2\pi\nu d\sqrt{\epsilon}$, with d the physical thickness and ν the frequency, which sets the transmission coefficient of a single disc, found to be $\mathcal{T} = i2\sqrt{\epsilon}/[i2\sqrt{\epsilon}\cos\delta + (\epsilon+1)\sin\delta]$. When $\delta = \pi, 3\pi, 5\pi, ...$, the disc is transparent ($\mathcal{T} = 0$) and the emission from different discs can be added constructively by placing them at the right distance. When $\mathcal{T} \neq 0$, the spacings can be adjusted to form a series of leaky resonant cavities where E-fields are boosted by reflections between the discs. In general both the simple sum of emitted waves and resonant enhancements are important.

3.2 Theoretical modelling of dielectric haloscopes, boost factor calculations

To see what a dielectric haloscope is capable of, we must study its general behavior. After choosing ϵ and the thickness of the discs d, the distances between discs remain as the only free parameters of our dielectric haloscope, still leaving considerable control over the frequency

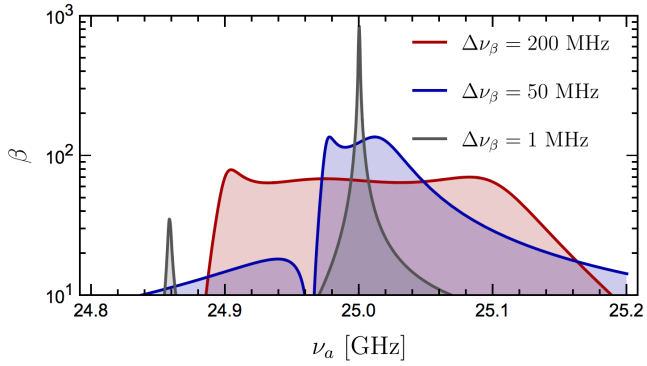

Figure 5. Boost factor $\beta(\nu_a)$ for configurations optimized for $\Delta\nu_\beta = 200$, 50 and 1 MHz (red, blue and grey) centered on 25 GHz using a mirror and 20 dielectric discs ($d = 1\,\text{mm}$, $\epsilon = 25$). Figure taken with permission from [10].

response. We will actually be interested in two types of configurations: one with a flat broadband response to measure a large frequency range in one go, and another with a larger β over a narrow band to discard statistical fluctuations and do precision axion physics in case of a discovery. The rational behind this approach is discussed in section 5. We can numerically generate such configurations.

One can predict the general behavior of β by using what we call the Area Law: $\int \beta^2 d\nu_a$ is proportional to the sum over interfaces, which holds exactly when integrating over $0 \leq \nu_a \leq \infty$, and is a good approximation for frequency ranges containing the main peak [51]. According to the Area Law, an increase in the number of discs gives a linear increase in $\int \beta^2 d\nu_a$. Conversely, for a single set of discs $\int \beta^2 d\nu_a$ is constant; one can trade width for power and vice versa, but cannot gain in both simultaneously. This is the main reason for our desire for rectangular responses: rectangles give the most efficient use of the available area.

To show the Area law in effect, Figure 5 depicts $\beta(\nu_a)$ for a dielectric haloscope consisting of a mirror and 20 discs ($d = 1$ mm, $\epsilon = 25$). Spacings have been selected to maximize the minimum boost factor β_{min} within three bandwidths $\Delta\nu_\beta = 1$, 50 and 200 MHz centered on 25 GHz (our benchmark frequency corresponding to $m_a = 103.1\ \mu$eV). As predicted by the area law, when we vary the bandwidth the power changes by roughly the same factor. While the area is conserved, it appears to be more effectively used in broadband configurations where we were able to obtain flatter $\beta(\nu_a)$ curves. Using the Area Law we extrapolate to the 80 disc setup described below, reaching $\beta_{\text{min}} \sim 275$ across 50 MHz. The achievable β_{min} changes with the optical thickness of a disc—in the example shown $\delta \sim 0.8\pi$, neither transparent nor fully reflective. Note that for a given d, there are frequency bands around $\nu_a = 1, 3, 5, ... \times \pi/(\sqrt{\epsilon}d)$ for which the discs are transparent and β is limited to the sum of the EM waves $\beta_{\text{min}} \leq 2N + 1$, where N is the number of discs. Further, at $\nu_a = 2, 4, 6, ... \times \pi/\sqrt{\epsilon}d$ the discs do not emit any radiation. Thus when large β or flexibility is required one must avoid these frequencies with a different set of discs.

The required disc positioning precision to obtain the desired rectangular shape can be estimated by studying those cases that can analytically be solved: the single cavity and the $\lambda_a/2$ symmetric case. For Gaussian positioning errors, a standard deviation of

$$\sigma \lesssim 20\,\mu\text{m} \left(\frac{10^2}{\beta}\right)^{1/2} \left(\frac{100\,\mu\text{eV}}{m_a}\right) \tag{3.5}$$

is required for $\lesssim 10\%$ error in β^2 [51].

4 Experimental ideas towards a realistic experiment

The basic principle of axion to photon conversion relies on the theoretical prediction that axions mix with photons in an external static magnetic field [45], as discussed above. The conversion of hidden photons to regular photons is based on the same principle but in this case no magnetic field is required [52]. During propagation of the wave, the axion (or hidden photon) part of the wave function is insensitive to boundaries at which there is a change in refractive index (dielectric constant). However, there is an effect to the photon part of the wave. This leads to emission of electromagnetic waves in both directions perpendicular to the dielectric surface (see Sec. 3).

4.1 The dish antenna approach

One of the simplest options for a broad band search experiment is to use only a mirror, possibly inside a magnetic field. With the approach to search for dark matter axions or (hidden photons) using only a (un)magnetized mirror, a frequency independent power, i.e. completely broadband output is obtained as long as radial size satisfies coherence conditions. This makes it easy to scan a large frequency range at once, if sensitive enough receivers are available for the given bandwidth. Therefore the dish antenna approach could be a comparably fast way to search for dark matter hidden photons and ALPs that could also test some important aspects of the dielectric haloscope approach. It is therefore interesting to investigate the reach of this method using the knowledge and infrastructure (prototype magnet, cryogenic facilities, receiver) devised for developing a dielectric haloscope approach. Even with relatively small mirror surfaces of the order $1\,\mathrm{m}^2$ it seems feasible to cover as of yet unexplored territories in the parameter space for darkmatter axions and hidden photons within a comparably short time scale [53]. The dish antenna appears like a quick and pragmatic approach to search for Axion Like particles.

4.2 The dielectric haloscope approach

For the search for dark matter axions the power boost β^2 of the dielectric haloscope can be used to enhance the axion induced photon emission within specific frequency intervals. This boost is coming from additional photon-emitting dielectric surfaces plus the "wave guide impedance transformation" resulting from interference effects in many dielectric vacuum layers. For a large boost factor it is necessary to match the free space impedance to the very low surface impedance of the mirror (impedance matching). In this case the dark matter axion experiment would consist of three main components:

- A dielectric structure consisting of a mirror and a significant number of thin ($\sim 1\,\mathrm{mm}$) discs of material with a high dielectric constant mounted parallel to the mirror surface. The position of the discs with respect to the mirror needs to be adjustable to high precision.
- A strong dipole magnet ensuring a magnetic field component parallel to the disc surfaces.
- A receiver that can detect a signal of order $10^{-23}\,\mathrm{W}$ power from a measurement with a bandwidth $\sim 50\,\mathrm{MHz}$ within $\lesssim 1$ week in the interesting frequency range (10–100 GHz).

4.3 Synergies between dielectric haloscope and dish antenna approaches

For axion masses $\gtrsim 400\,\mu$eV the dielectric haloscope approach loses sensitivity due to two effects:

- The axion de Broglie wavelength becomes similar to the size of the experimental setup leading to a loss of coherence.
- The required average disc spacing becomes smaller than $\sim 3\,$mm, which is challenging to obtain for a many disc setup with diameter ~ 1 m^2 due to mechanical constraints.

Any receiver developed for the dielectric haloscope approach can also be used in a dish antenna setup. In fact, a dielectric halocsope without any dielectric discs corresponds to a dish antenna setup. While the sensitivity in this case will be reduced by the power boost factor of the booster, such a setup could potentially already allow at a significantly earlier stage for sensitivity in unexplored regions in the parameter space for hidden photons and ALPs if a prototype magnet is already available. For the search of QCD axions the sensitivity will have to be boosted either by the dielectric haloscope method or by significantly reducing the noise temperature of the system (see eq. 5.1 below).

5 Baseline design: Proposed experimental setup for the search of dark matter axions

5.1 MADMAX design

We propose here the MAgnetized Disc and Mirror AXion (MADMAX) experiment [54], which would exploit the dielectric haloscope approach described above [10, 51].

As described in sec. 3, for coherent interaction of the axion with the experimental setup the integral under the power boost factor $\beta^2(\nu)$ scales linearly with the number of magnetized discs, N, as well as increasing with the dielectric constant [51] up to $\epsilon \sim 100$. Thus, the sensitivity of a setup can be scaled up by increasing the number of discs and using a material with high ϵ. In other words, the photon power emitted by a dielectric haloscope can be scaled to a value of $\sim 2\times 10^{-23}\,$W, detectable by state of the art radiometers in the frequency range ∼10–30 GHz if β^2 exceeds $\sim 10^4$.

Electromagnetic simulations have revealed that configurations with $\beta^2 \sim 2500$ can be achieved for $\Delta\nu \sim 250\,$MHz, using 20 plates of $LaALO_3$ with ϵ=24. Fig. 6 shows the power boost factor as a function of frequency resulting from these simulations. For each configuration 250 simulations were performed with Gaussian variations of the discs spacings with a precision of σ=10 μm. This indicates that variations due to 15 μm positioning uncertainties are not significant in this frequency range.

The power boost frequency range can be seamlessly shifted by changing the spacings between the discs. In addition, as shown above the bandwidth of the boost factor curve can be adjusted. The area law then implies that for a narrower bandwidth setting a higher power boost β^2 can be achieved.

Using the scaling laws described above, a setup with 80 discs with area $\sim 1\,$m^2 in a magnetic dipole field of 10 T would be sufficient to boost the photon emission of the haloscope to a detectable level. For a realistic setup with a reasonable size the average distance between the discs could range between a few mm (high frequency range) and a few cm (low frequency range).

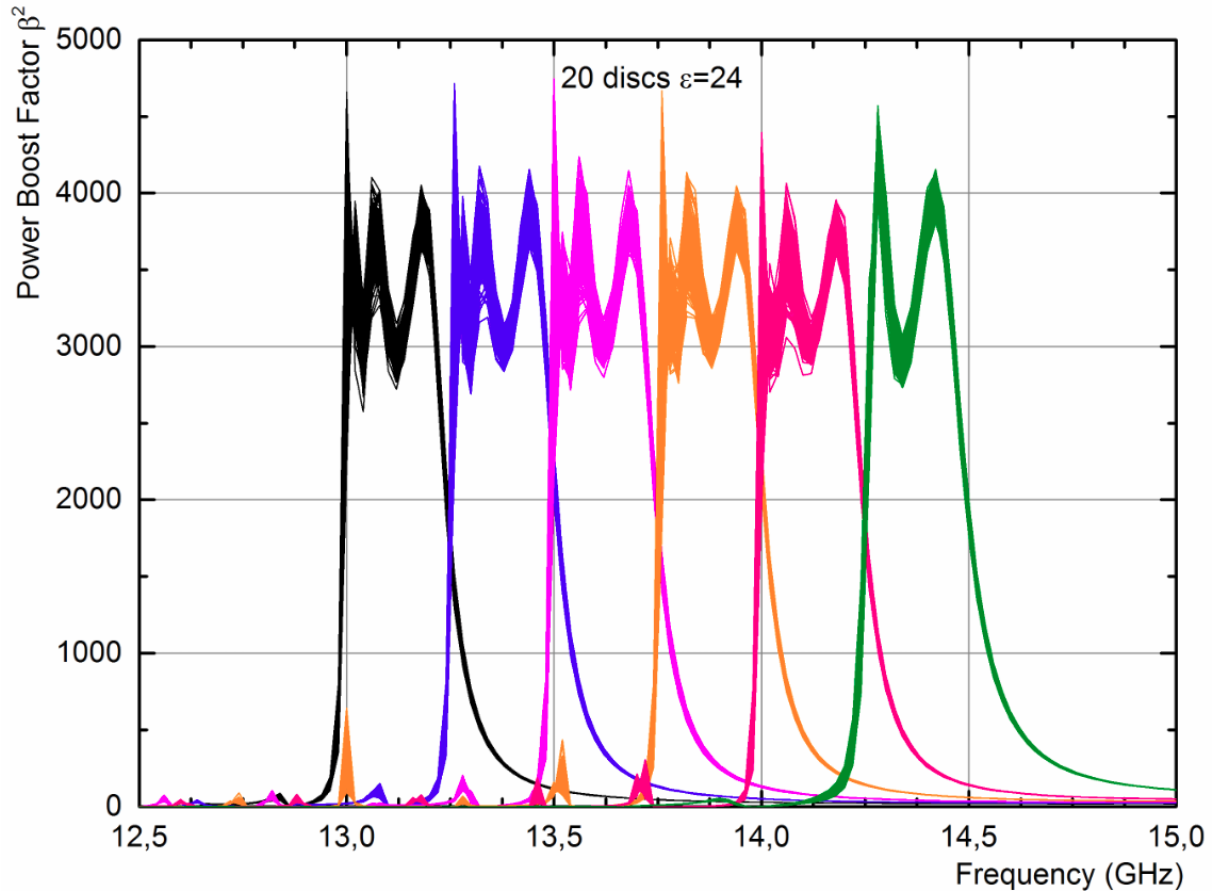

Figure 6. *Simulations of boost factor with 20 $LaAlO_3$ discs (ϵ=24) for six different disc spacing configurations. For each configuration a power boost factor of $\sim$ 2500 is achieved over a bandwidth of $\sim$ 250 MHz. The 250 simulations performed with random Gaussian variations of the discs spacings with a precision of σ=15 μm are plotted above each other.*

Such a setup would be sensitive to dark matter axions in the $40-400\,\mu$eV range, covering a good fraction of the predicted axion mass range in the post inflationary PQ scenario.

A schematic of the proposed MADMAX approach is shown in Fig. 7. The experimental setup can be divided into the three main components:

- The dipole magnet with $\sim 1\,\mathrm{m}^2$ aperture, ensuring the $\sim 10\,\mathrm{T}$ magnetic field,
- The booster, consisting of a mirror at the far end and the ~ 80 dielectric discs that can be positioned within a few μm precision by motors,
- The receiver, including the parabolic mirror and the feedthroughs, which is used for detection of the emitted power.

It is clear that this sketch can only be a first guess for a realization. The detailed design will depend on the findings of investigations of remaining questions (discussed below). It needs to be optimized once satisfying answers to these questions have been obtained.

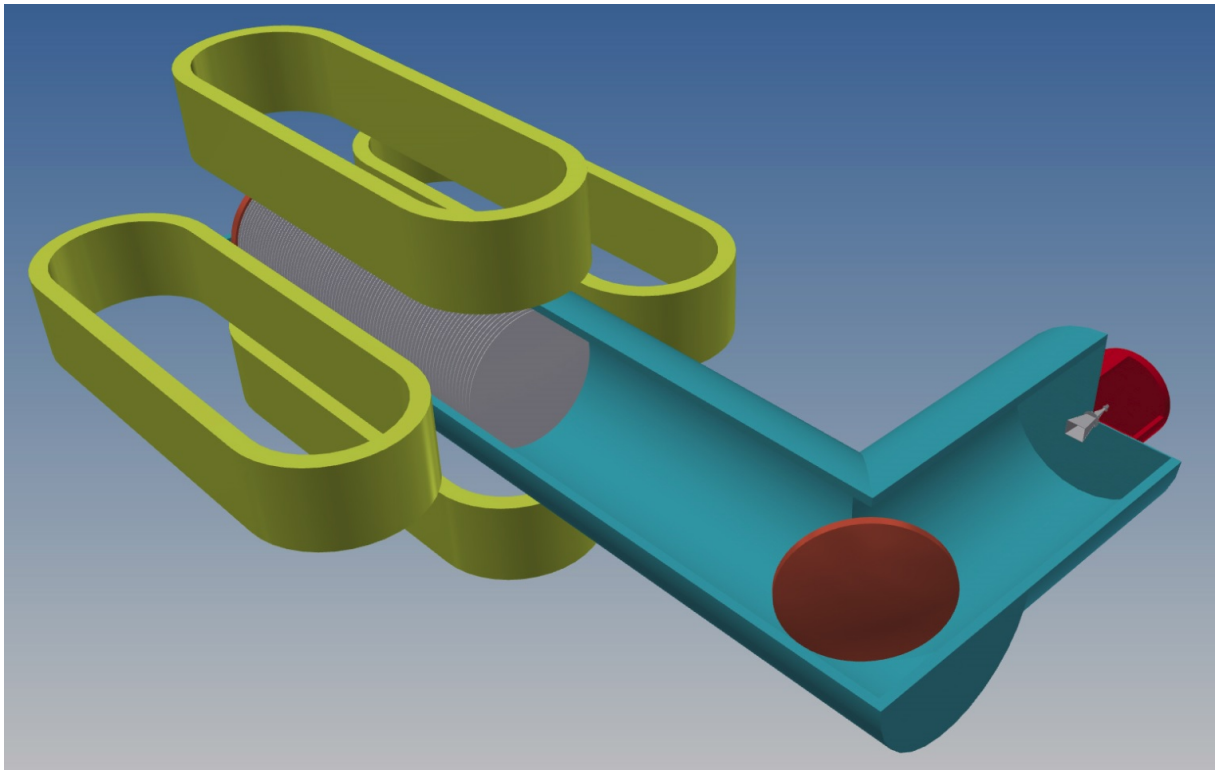

Figure 7. *Baseline design of the MADMAX approach. The experiment can be divided into three parts: 1) magnet (yellow racetracks), 2) booster – consisting of the mirror (copper disc at the far left), the 80 dielectric discs (gray) plus parabolic mirror (copper disc at the right) and the system to adjust disc spacing (not shown) – 3) the receiver – consisting of the horn antenna (gray) and the cold preamplifier inside a separated cryostat (red).*

5.2 The magnet

The photon–axion conversion at dielectric transitions scales with the magnetic field component parallel to the surface B and the surface area A as B^2A. When designing a magnet for the haloscope it is this quantity that should be maximized while the maximum length for the setup given by coherence issues, signal attenuation in the discs and mechanical constraints are considered. From the estimations above a magnet suitable for the experiment should reach at least $100\,T^2m^2$ over a length of up to $\sim 200\,cm$. Presently two design concepts that seem feasible are discussed. They are based on the Canted Cosine Theta magnet design [55] and on a race-track design [56]. In order to verify the feasibility of the concepts and to potentially identify different magnet approaches, design studies are being ordered. These should reveal the time and cost scales of the proposed magnets within the next year.

5.3 The booster

Depending on the size of the magnet, it will be necessary to use up to 80 discs placed inside a magnetic field with strength $\sim 10\,T$. According to eq. 3.5 the mean distances between the discs, ranging from $\sim 20\,mm$ at 10 GHz to $\sim 2\,mm$ at 100 GHz will have to be aligned with a precision of about $10\,\mu m$ and $1\,\mu m$, respectively. For 80 discs this would necessitate a length of the system of up to 200 cm (low frequency setup). The booster could consist of framed discs with thickness $\sim 1\,mm$, connected to precision rails on which they can be moved by a mechanism connected

to precision motors. While the precision of the pistons of motors can be easily controlled to the sub μm level, the mechanical transmission from motors to discs in a high magnetic field and cryogenic environment as well as gravity can lead to sizable uncertainties in the exact disc positioning. The technology to ensure in-situ adjustable disc spacing with high enough precision in the experimental surrounding with 10 T magnetic field and cryogenic ambient temperature needs to be developed.

Any material used as dielectric in the experiment has to fulfil the following criteria:

- High dielectric constant $\epsilon \gtrsim 10$
- Low dielectric loss $\tan\delta \lesssim 10^{-4}$,
- Mechanically stable,
- Appropriate cryogenic properties down to 4 K,
- Affordable.

Presently $LaAlO_3$ is envisioned as the baseline candidate for its high dielectric constant and low dielectric loss also at low temperatures [57]. The technology to produce sufficiently large discs with high enough precision ($\sim \mu$m) needs to be developed. Alternative materials could be Al_2O_3 [58] or TiO_2 (Rutil) [59].

Another important task will be to understand and control the influence of the booster and its surrounding on the noise temperature of the receiver. In order to reach the goal of a total system noise temperature T_{sys} of 8 K (see below, eq. 5.1) with a preamplifier noise temperature of 6 K, the added noise needs to be less than $\sim$2 K.

5.4 Heterodyne mixing and the receiver

The proposed principle of microwave detection, at least for the frequency regime below $\sim$30 GHz, is based on heterodyne mixing of a preamplified signal [60]. This is sketched in Fig. 8. After the first low noise preamplifier stage (HEMT) and pre-filtering, the signal is twice shifted to intermediate frequencies by mixing a carrier frequency into the signal. At the intermediate frequencies the signal is further amplified and filtered. Finally, the signal is at a frequency that is accessible to digital 16 bit samplers, which have internal FPGAs that provide real time fast Fourier transform calculation and the subsequent integration and storage of the signal.

As mentioned above, state of the art detector technology requires different systems for the frequency ranges 10–30 GHz and above 30 GHz. For the first frequency range HEMT detectors [61], as widely used in, for example, the radio astronomy community , can be used. For the baseline design we propose HEMT receivers from Low Noise Factory[3] for the lower frequency range (10–30 GHz). For the high frequency range new detectors working at the quantum noise limit still have to be identified and developed.

5.5 Expected sensitivity and measurement strategy

The expected sensitivity of the setup is based on the following assumptions:

- Availability of receiver system with noise temperature of few K, i.e. so a signal power of $\sim 10^{-23}$ W for an axion line width of $10^{-6}\,\nu_a$ can be detected within few days within a frequency range of $\sim$50 MHz and a significance of $\gtrsim 4\sigma$.

[3] www.lownoisefacory.com

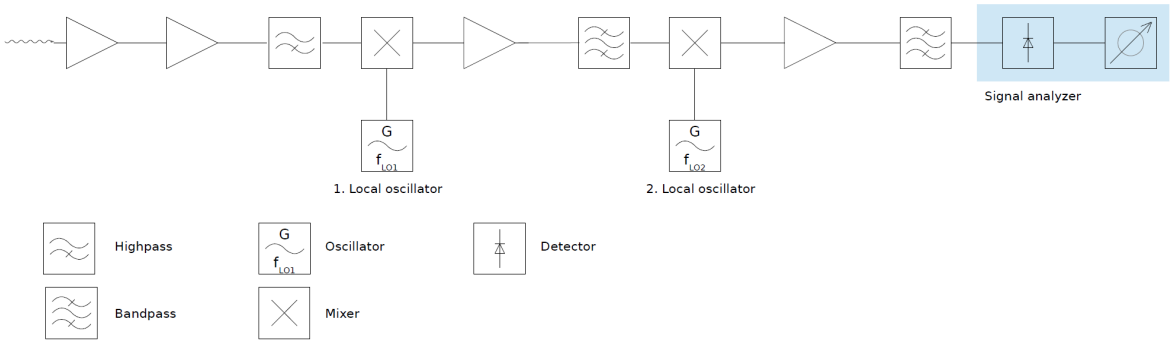

Figure 8. *Sketch of signal processing steps. For more details see text.*

- A booster with ~ 80 discs with area $\sim 1\,\mathrm{m}^2$ can be built that ensures a power boost of $\gtrsim 10^4$ across a frequency range of $\sim 50\,\mathrm{MHz}$
- A magnet with large enough aperture and length to house the booster can be built, that ensures an integrated magnetic field $\sim 100\,\mathrm{T}^2\mathrm{m}^2$ parallel to the booster disc surfaces.
- The overall measuring time for a single frequency range with bandwidth $\sim 50\,\mathrm{MHz}$ is a few days. Additionally we assume that re-measurement with readjusted discs spacings resulting in higher boost at those regions that yielded evidence for a signal is possible. Interruptions due to readjustment time of the discs have to be included.

The sensitivity can then be calculated using Dicke's radiometer equation [62],

$$\frac{S}{N} = \frac{P_{\mathrm{sig}}}{k_B T_{\mathrm{sys}}} \sqrt{\frac{t_{\mathrm{scan}}}{\Delta\nu}} \tag{5.1}$$

where k_B is the Boltzmann constant, T_{sys} the total system noise temperature, P_{sig} is the signal power, t_{scan} the scanning time for an individual measurement and $\Delta\nu = \nu\Delta a = 10^{-6}\nu$ the predicted axion line width at given frequency ν. Note that the sensitivity for a dish antenna approach with a $1\,\mathrm{m}^2$ magnetized dish is given by the sensitivity for the MADMAX design without any boost ($\beta = 1$).

The sensitivities obtainable with the MADMAX approach for dark matter axions and hidden photons with a mass between 40 and 400 μeV are shown in Figs. 9 and 10, respectively. A significant part of the parameter space predicted for dark matter axions in the post inflationary Peccei Quinn scenario could be probed. Also a parameter space consistent with hidden photons as dark matter could be probed down to kinetic mixing angles of a few times 10^{-16}. The time needed to scan the indicated frequency ranges will be discussed below.

In Fig. 9 we also show the sensitivity for dark matter axions and for hidden photons that can be obtained using just the magnetized mirror, with a $1\,\mathrm{m}^2$ surface in a 10 T field (for the axion case), after either 1 week or 5 years of measurement with a 8 K system noise temperature device. In the axion mass range between 40 and 400 μeV both are more than an order of magnitude less sensitive than an 80 disc dielectric haloscope. However, for masses below $\sim 40\,\mu$eV or above $\sim 400\,\mu$eV a dish antenna could be used to investigate unexplored areas in the parameter space.

The measurement strategy depends on the sensitivity of the detection system, i.e. the measurement time required to detect a $\sim 10^{-23}\,\mathrm{W}$ signal with high enough significance. Additionally

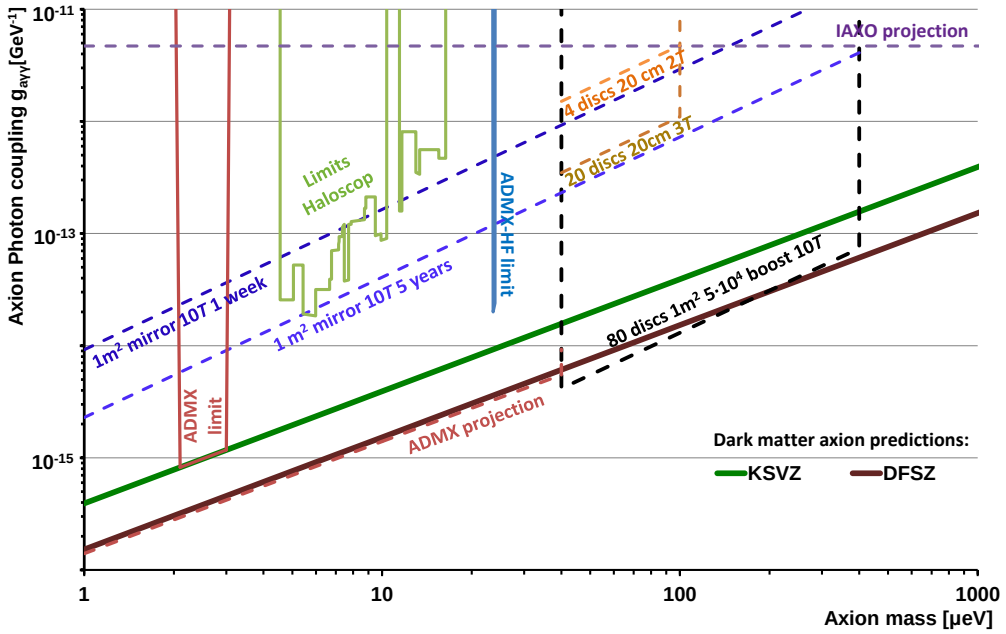

Figure 9. *Projection of sensitivities for dark matter axions and ALPs in the coupling vs. mass parameter space. The model dependent predicted mass of dark matter axions in this representation lies on the lines denoted DFSZ and KSVZ referring to the two most accepted models. For all limit setting sensitivities an axion line width of 10^{-6}, 8 K total noise temperature of the benchmark system and 4 σ separation from background have been assumed. For the MADMAX projection an 80 dielectric discs with 1 m^2 area setup in 10 T magnetic field strength parallel to the discs have been assumed. Also shown are sensitivity projections for prototype setups with 4 and 20 discs with 20 cm disc diameter in 2 T and 3 T magnetic fields and for a pure magnetized dish approach after one week and five years of measurement. The projected sensitivities are compared to existing limits from ADMX and other haloscope experiments [63], from ADMX-HF [3]. Also the IAXO [64] sensitivity for solar axions and ALPs is indicated.*

it will depend on the time needed to readjust the disc spacings with high enough precision in order to change the power boost factor curve, i.e. either the bandwidth of the curve or the frequency range in which the power boost is enhanced.

Scanning through the frequency range is planned according to the following procedure:

- Position discs such that the boost factor curve has the desired "broad" (~ 50 MHz) bandwidth.
- Take data until the predicted dark matter signal for the given mass range could be detected within the probed bandwidth with a given probability P_1 (to be defined).
- Re-measure all candidate signal within "broad" bandwidth using disc positionings resulting in narrow boost factor curve around the candidate signals. Using this higher expected signal one would data until the probability required for detection of signal $P_2 > P_1$ is reached.

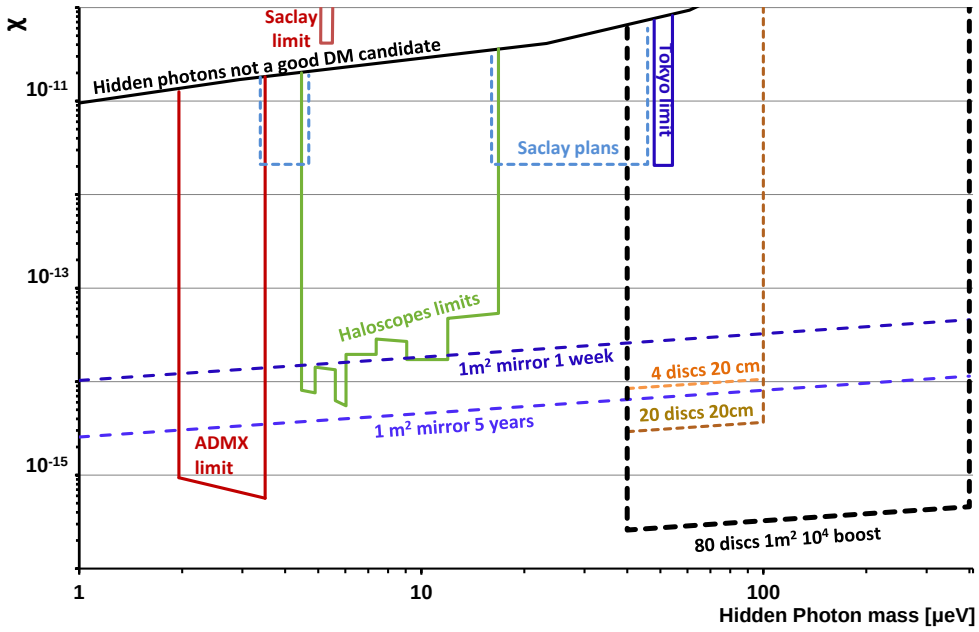

Figure 10. *Projection of sensitivities for hidden photons. For all limit setting sensitivities a hidden photon line width of 10^{-6}, 8 K total noise temperature of the system and 4 σ separation from background have been assumed. For the MADMAX projection, a setup using 80 dielectric discs with 1 m^2 area have been assumed. Also shown are sensitivity projections for prototype setups with 4 and 20 discs with 20 cm disc and for a pure dish approach after one week and five years of measurement. The projected sensitivities are compared to existing limits from ADMX and other haloscope experiments for hidden photon search from [52]), from ADMX-HF [3] and from the latest Tokyo results [65]. The limit obtained with a first simple setup at Saclay and a projection of the sensitivity of a setup in preperation at Saclay are also shown. The area above the black line [52] represents the parameter space where hidden photons are not a good dark matter candidate.*

- Reposition discs to next "broad" frequency range and repeat until the desired parameter space is searched or one gets a detection.

The time needed to cover 1 GHz bandwidth as a function of obtainable power boost factor and the confidence level to which in the first round a signal should appear is shown in Fig. 11. Here it was assumed that the readjustment time for the discs is one day (during which no data is taken). This is a conservative estimate and it is likely to be less, especially if only a slight adjustment of the frequency range is needed.

As seen from the plot, if a power boost of 2×10^4 can be reached, the time needed to scan one GHz would be $\sim$80 days. I.e. the frequency range 10–30 GHz, corresponding to axion masses between 40 and 120 μeV could be scanned within $\sim$5 years.

5.6 Experimental site considerations

For the site where the experiment could be built a few boundary conditions need to be met:

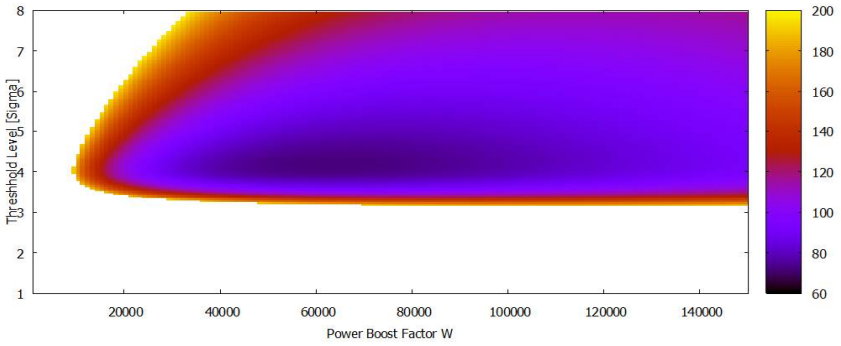

Figure 11. *Time in days needed to scan 1 GHz frequency range as a function of power boost obtainable and preset confidence level for the search.*

- Availability of infrastructure: Sufficient power and cryogenic infrastructure to cool the magnet, the booster surrounding and the detection system to their operational temperature of $\sim 4\,\mathrm{K}$ is required. Additionally a workshop in the near surrounding of the experiment would be beneficial.
- Accessibility: easy access and cranes for inclusion of big parts, especially for the magnet is needed.
- Low enough electromagnetic background environment in the microwave regime: Noise levels of $\lesssim$,-130 dBm below 10 GHz and $\lesssim$-180 dBm above 10 GHz are necessary at the place of measurement. Good EM enclosures can damp external signals by $\sim 80\,\mathrm{dB}$. Thus the background requirements are $<$-50 dBm in the frequency range below 10 GHz and $\lesssim$-100 dBm above 10 GHz.
- Sufficient space: The whole final dielectric haloscope setup, which would have dimensions up to $\sim$5 m in diameter and $\sim 5\,\mathrm{m}$ in length, the shield against the fringe magnetic field, cryogenic and vacuum infrastructure as well as the shielded electronics must fit. This would require a total space of $\sim 1000\,\mathrm{m}^2$.

The detailed requirements will be investigated in the first phase of the experiment.

6 Proof of principle measurements with first test setup

First proof of principle systems for the booster and the receiver have been assembled already. The setup of the proof of principle booster is shown in Fig. 12 (left). The shown configuration consists of five sapphire (Al_2O_3 with $\epsilon \sim 10$) discs each with 200 mm diameter. The discs can be positioned by precision motors to a precision better than 15 μm. The maximum translation of the motors is 25 mm. Here the primary uncertainty on positioning is due to the force transmission rather than the limitations of the motors.

Alternatively the setup can be equipped with one mirror (a copper plate with high precision surface) at the far end and four discs for reflectivity measurements.

A receiver system based on a HEMT preamplifier and heterodyne mixing as described above has been set up. Data acquisition happens through four digital 16 bit samplers with internal FPGAs that ensure real time FFT calculation and subsequent integration of the signal. Using

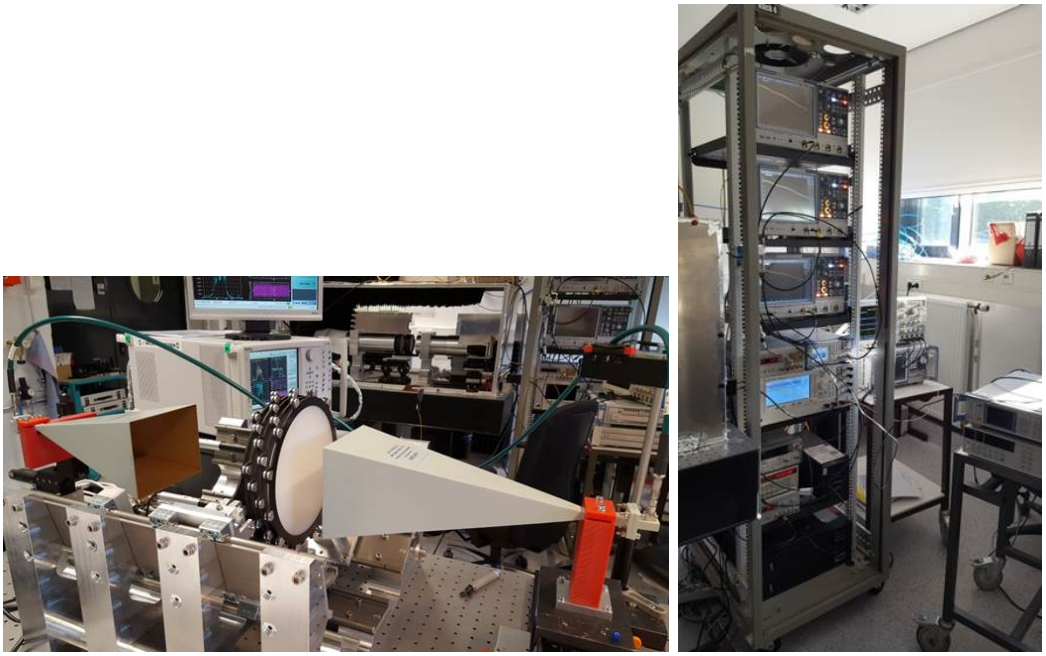

Figure 12. *Left: Proof of principle setup for transmission measurements with five discs. Right: receiver system*

four samplers reduces the dead time of the system due to internal signal conversion and memory storage from 75% to less than 2%.

The setup described above was used for first proof of principle measurements. These measurements indicate that the assumptions on 10–30 GHz receiver sensitivity and disc placement precision, necessary to estimate the sensitivity of the MADMAX approach are realistic. Some details on these measurements are described in this section.

6.1 HEMT preamplifier measurements

First measurements with the HEMT preamplifier performed inside liquid helium have been performed. The gain and noise behaviors are shown in Fig. 13. While the gain as function of frequency was confirmed to behave as expected from the data sheet, the measured noise was higher by $\sim 2\,\mathrm{K}$ with respect to expectations from the data sheet. This is attributed to the non-optimal preliminary setup inside a liquid helium transport dewar.

To determine the required signal strength, the receiver system described above was used for measurement of a weak signal ($\sim\ 5 \times 10^{-23}$ W) at 17.8 GHz with a sampler bandwidth of 50 MHz with a Fourier transform bin-width of 2 kHz and the preamplifier inside liquid helium. The injected signal corresponds to a photon flux with bandwith of 10^{-7} of the freequency (instead of $10^{-6} as expected from an axion signal$ of 4.2 photons per second. The fake axion signal could be detected within three days measurement time with $\gtrsim 4\,\sigma$ separation from background.

6.2 Transmissivity and Reflectivity measurements

The axion (or hidden photon) to photon conversion can be treated classically: it simply sources an additional term in the Maxwell equation (see sec. 3). This implies that transmissivity and reflectivity of the haloscope can be calculated for a given boost factor curve. Hence, they can be

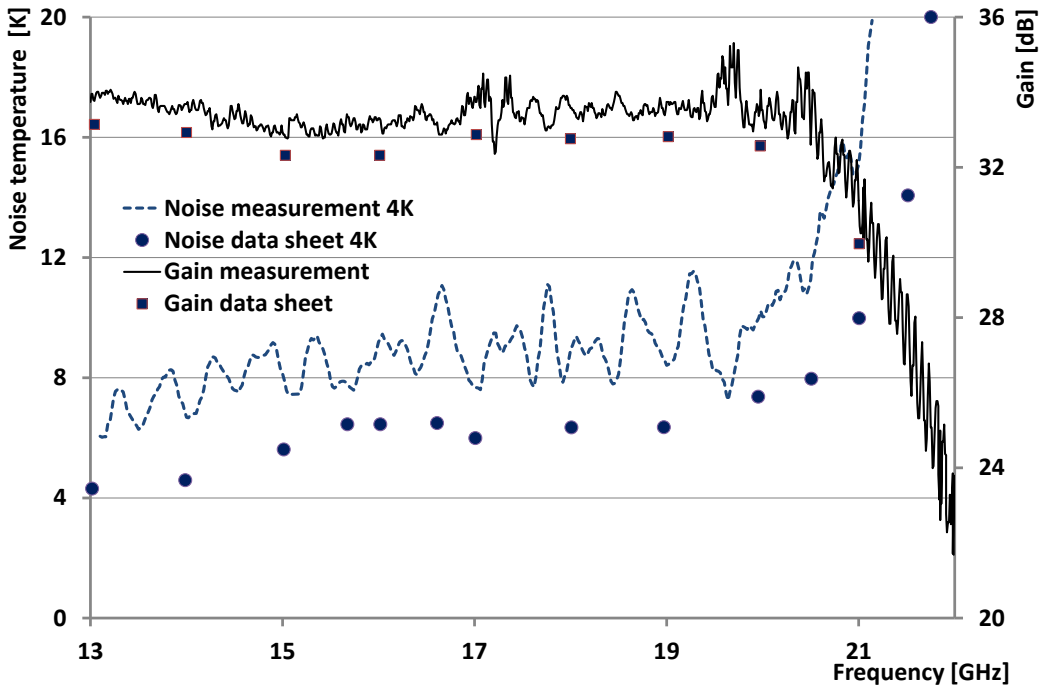

Figure 13. *Gain and noise measurements of the HEMT preamplifier at 4.1 K. Expectations from the data sheet are also shown.*

used to verify the simulated boost factor behavior. This is used to test the calculations of the boost factor and to aid correct disc placement. This has been done with the prototype setup shown in Fig. 12.

In general for the group delay distribution one expects as many peaks as there are discs, while for the transmissivity there appears one peak less than there are discs in the setup. For both curves the peak at highest frequency has the highest correlation with the expected boost factor curve.

A comparison of a transmissivity measurement with 1-D simulation is shown in Fig. 14. While details of the transmissivity behaviour differ slightly, the general behaviour is encouragingly similar, especially the position of the peak at highest frequencies, which has the highest correlation with the boost factor curve. The same has been consistently verified for reflectivity measurements using group delay peaks.

The long term stability was investigated using a long term ($\sim$15 hours) reflectivity measurement with four sapphire discs and a metallic mirror. The variations of the peak position, attributed to mechanical (vibration) or thermal (contraction or expansion) changes in the setup, are of the order of 1 MHz, substantially narrower than the envisioned bandwidth of the boost factor. This proves that long-term measurements can be performed over a sizeable bandwidth even under these experimental conditions (without vibrational damping and temperature fluctuations of the order $\pm 1^0$ C).

In order to improve the match between measurement and simulation, an algorithm is being developed for disc placement:

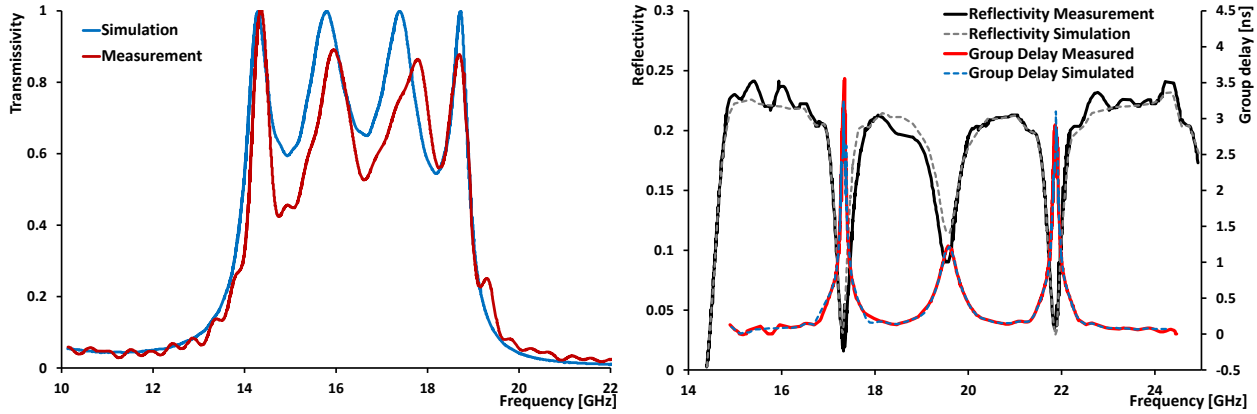

Figure 14. *Left: First smoothened transmission measurement (red) taken with five manually adjusted Al_2O_3 discs between receiver and emitter compared to the behavior predicted by simulation (blue). Right: reflectivity (black) and group delay (red) measurements as compared to simulation for a 3 disc setup after optimization of disc spacings using an iterative algorithm.*

- A reflectivity measurement is done.
- Group delay and reflectivity are compared to the ones calculated for the given boost factor curve. The algorithm calculates a set of disc positions with which a better agreement between measurement and expectation can be obtained.
- The discs are positioned to this new set of coordinates.
- The reflectivity and group delay measurements are repeated.
- This is done iteratively until the positions converge and the difference is tolerably small.

Fig. 14 (right) shows for a preliminary realization of the algorithm using a three disc plus mirror setup the comparison of measured and simulated reflectivity and group delay as a function of frequency after optimization. With the current algorithm typically convergence happens after ~ 30 iterations, with a very good match between the two spectra. The specification on the accuracy of disc thickness is 25 μm. In order to get the best match between simulation and measurement the disc thickness used for the simulation had to be adjusted within the uncertainty range. For several attempts the reproducibility of the individual disc positions was within 1 μm. This gives confidence that the precision can be well controlled, at least for 20 cm discs.

7 Towards realization of MADMAX: magnets, prototypes and sites

It is encouraging that the receiver sensitivity and the precision of disc placement could be verified experimentally for a 20 cm diameter, four disc plus mirror setup. Before a full scale experiment can be built, however, additional investigations have to be performed.

- The proposed components have to be tested for their performance in a strong magnetic field.
- A technology to obtain dielectric disc areas of $\sim 1\,\mathrm{m}^2$ has to be developed and tested.

- The obtainable precision of disc placement inside strong magnetic field in vacuum and at cryogenic temperatures has to be studied.
- The scaling behavior of the power boost with the number of discs and their area has to be investigated.
- The system noise behavior has to be studied down to temperatures around 4 K.

It will be necessary to build a magnet test-infrastructure and prototypes of the dielectric disc structure.

It is planned to implement a magnet for component testing that allows to investigate the behavior of the different components to be used in the experiment inside a strong ($\sim$8 T) magnetic field. Additionally it is planned to build a dipole magnet with 3–4 T field with sufficiently large volume to house several prototype setups inside. This setup would be flexible enough to host prototypes of different size, also in cryogenic environment.

Prototype setups with smaller dimensions and reduced number of discs will be built to investigate the scaling behavior of the individual components. This setup will be used to study adjustment of disc positions for a defined frequency and bandwidth. The algorithm to find the right disc configuration will be adjusted for a system containing many discs. The setup will designed so it can later be implemented into a cryogenic surrounding that can be moved into a magnet to repeat the measurements inside a strong magnetic field.

The cryogenic performance of the mechanical parts will be studied in a dedicated cryostat that allows the components to be cooled down to 4 K. For understanding of the total system temperature a cryostat will be needed that allows one to cool the prototype dielectric disc setup down to 4 K.

The north hall at DESY could be a candidate site for the experiment. It fulfills the space and infra structural requirements and is $\sim$20 m below the surface. It has enough overburden to sufficiently shield anthropogenic and natural electromagnetic radiation present at the surface. First background measurements at the site in the frequency range between few Hz and $\sim$20 GHz have been performed. Above 1 GHz the measured background consistently had a level $<$ -100dBm; no signal could be detected. Between 100 MHz and 1 GHz some signals from radio stations, telecommunication and emergency communication transmitters are present, but also in this frequency range the general noise was consistently less than -100 dBm. No correlations with RF activities of the PETRA and FLASH RF infrastructure—ongoing during the measurements—were found. These first measurements indicate that DESY might be a potentially interesting site. More long term measurements are required to qualify the site as an experimental site.

8 Physics reach with prototypes

Already with a prototype setup physics results could be achieved. As shown in Fig. 9, with a setup consisting of 4 discs with 20 cm diameter in front of a mirror inside a 2 T magnetic field a sensitivity could be achieved that exceeds the projected sensitivity of the proposed IAXO experiment for solar axions [64] in this mass regime. A setup with 20 discs in a 3 T magnetic field could already have a sensitivity exceeding the one of a dish antenna experiment after 5 years in a B field of 10 T.

Even without a magnet, a prototype setup could considerably improve the existing limits in the search for dark matter hidden photons and so cut into unexplored territory in the allowed

parameter space. Even a four disc setup would improve the limit obtained by the Tokyo group for $\sim$ 50 μeV hidden photons [65] by more than two orders of magnitude. A much simpler device with room temperature pre-amplification could result in coverage of parameter space complementary to the ADMX and other microwave cavity searches as well as the Tokyo results within a relatively short timescale (see projections labelled Saclay plans in Fig. 9).

9 Timeline

As first steps it is planned to answer strategically important questions that have the potential to influence the design of the experiment. This will be done within the next 3–4 years using the test infrastructure and prototype setups described above. During this time also a feasibility study on the magnet technology will be performed and as a result a first realization of a prototype magnet is planned. Already during this time physics results could be achieved.

Based on the results from the prototype studies a final design will be devised. Presently it seems feasible to start building the final experiment starting in the year $\sim$2021 and start data taking in $\sim$2022. This would allow to probe the axion dark matter mass range between $\sim$40 and 100 μeV. During this time new detection techniques with quantum limited detectors would be developed to allow the sensitivity range of the experiment to be extended up to axion masses $\sim$400 μeV.

10 Conclusions

Axions are very well motivated particle candidates that could explain both the strong CP problem and the dark matter problem simultaneously. Their coupling to photons through the Primakoff effect makes them detectable in principle in the laboratory. This has been and is being exploited in experiments making use of resonant axion to photon conversion in cavities. These experiments are sensitive enough to probe axions as dark matter candidates in the axion mass range below $\sim$40 μeV. The axion mass range above 40 μeV, which is preferred in theoretical models where the Peccei-Quinn symmetry breaking occurs after inflation, is not yet experimentally explored.

We propose a new experiment, MADMAX, based on an extension of the dish antenna approach: a dielectric haloscope. We have shown that simulations and first experimental tests of the concept are very promising. This leads us to the conclusion that it is experimentally feasible to exploit this approach by extrapolating the results that were obtained with a small setup to a size that mechanically still seems feasible. We introduced the baseline design of the MADMAX experiment. This consists of three main components:

1. A booster with 80 discs with area $\sim 1\,\mathrm{m}^2$ made from material with high dielectric constant and low dielectric loss in front of a mirror. The distances between the discs need to be adjustable in a range from $\sim$2mm to $\sim$ 20 mm with a precision of a few μm.

2. A magnet with an aperture to fit the booster. The magnetic field parallel to the discs needs to be of the order 10 T.

3. Receivers that can detect microwaves with a power of $\sim 10^{-23}$ W in the regime 10 GHz to 100 GHz.

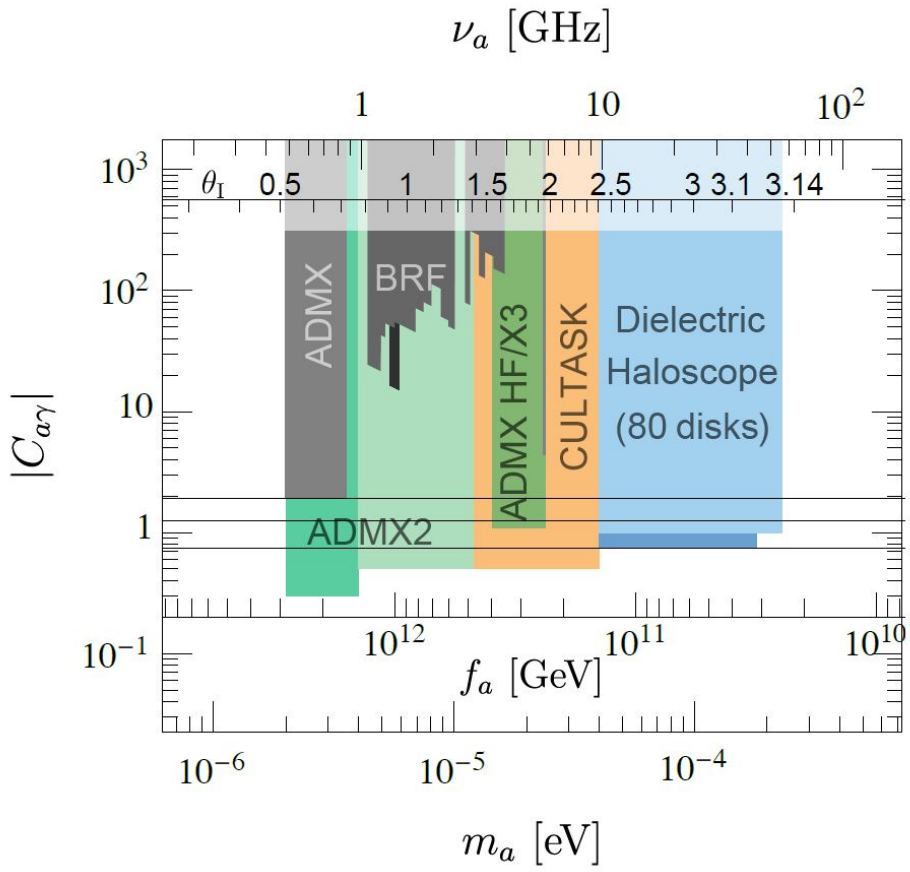

Figure 15. *Sensitivity of the MADMAX approach compared to other ongoing and future experimental projects.*

The whole setup needs to be installed in a surrounding with low electromagnetic noise. Presently the HERA hall north at DESY, Hamburg is discussed as a possible site.

In the next 2–3 years in a first step smaller prototypes for booster magnet with disc diameters of $\sim 30\,\mathrm{cm}$ will be designed and produced. These will allow us to verify the scalability of the technologies investigated so far. Such a setup would already allow to produce competitive results in the search for axion like particles and hidden photons.

Once the prototype is commissioned, improvements of the baseline design—based on the experience with the prototype—and building of the final experiment could start. In case of a smooth implementation, first measurements with a sensitivity high enough to probe dark matter axions could be taken starting from 2022. It would need roughly ten years to probe the whole mass range between 40 and 400 μeV predicted for axion dark matter in the case of Peccei Quinn symmetry breaking after inflation. This proposal presents the so far only known approach to cover this very well motivates mass range for axions and is, as shown in Fig. 15, very complementary to other axion dark matter searches discussed in literature.

11 Acknowledgments

The prototype setup used for first measurements was partly funded as a seed project by the DFG Excellence Cluster Universe (Grant No. EXC 153).

References

[1] G. Raffelt, Lecture Notes Phys. **741**(2008)51

[2] S. Asztalos et al., Phys. Rev. D **69**(2004)011101

[3] B. Brubaker et al., [arXiv:1610.02580]

[4] M. Kawasaki, K. Saikawa and T. Sekiguchi, [arXiv:1412.0789]

[5] T. Hiramatsu, M. Kawasaki, K. Saikawa and T. Sekiguchi, Phys. Rev. D **85**(2012)105020, Erratum ibid. **86**(2012)089902

[6] E. W. Kolb and I. I. Tkachev, Phys. Rev. D **49**(1994)5040.

[7] K. M. Zurek, C. J. Hogan and T. R. Quinn, Phys. Rev. D **75**(2007) 043511

[8] S. Borsanyi et al., Nature **539**(2016)69

[9] G. Ballesteros, J. Redondo, A. Ringwald, C. Tamarit, [arXiv:1610.01639]

[10] The MADMAX working group, A. Caldwell et al., Phys. Rev. Lett. , in print , [arXiv:1611.05865]

[11] D. Horns, J. Jaeckel, A. Lindner, A. Lobanov, J. Redondo and A. Ringwald, JCAP **1304**(2013)016 [arXiv:1212.2970].

[12] J. Jaeckel and J. Redondo, Phys. Rev. D **88**(2013)115002 [arXiv:1308.1103]

[13] J. E. Kim and G. Carosi, Rev. Mod. Phys. **82** (2010) 557 [arXiv:0807.3125 [hep-ph]].

[14] C. A. Baker *et al.*, Phys. Rev. Lett. **97** (2006) 131801 [hep-ex/0602020].

[15] R. D. Peccei and H. R. Quinn, Phys. Rev. Lett. **38** (1977) 1440.

[16] R. D. Peccei and H. R. Quinn, Phys. Rev. D **16** (1977) 1791.

[17] M. Pospelov and A. Ritz, Annals Phys. **318** (2005) 119 [hep-ph/0504231].

[18] C. Vafa and E. Witten, Phys. Rev. Lett. **53** (1984) 535.

[19] G. Grilli di Cortona, E. Hardy, J. Pardo Vega and G. Villadoro, JHEP **1601** (2016) 034 [arXiv:1511.02867].

[20] J. E. Kim, Phys. Rev. Lett. **43** (1979) 103.

[21] M. A. Shifman, A. I. Vainshtein and V. I. Zakharov, Nucl. Phys. B **166** (1980) 493.

[22] M. Dine, W. Fischler and M. Srednicki, Phys. Lett. **104B** (1981) 199.

[23] A. R. Zhitnitsky, Sov. J. Nucl. Phys. **31** (1980) 260 [Yad. Fiz. **31** (1980) 497].

[24] R. D. Peccei, T. T. Wu and T. Yanagida, Phys. Lett. B **172** (1986) 435.

[25] L. M. Krauss and F. Wilczek, Phys. Lett. B **173** (1986) 189.

[26] L. Di Luzio, F. Mescia and E. Nardi, Phys. Rev. Lett. **118**, no. 3, 031801 (2017) [arXiv:1610.07593].

[27] G. Ballesteros, J. Redondo, A. Ringwald and C. Tamarit, Phys. Rev. Lett. **118** (2017) no.7, 071802 [arXiv:1608.05414].

[28] T. Goto and M. Yamaguchi, Phys. Lett. B **276** (1992) 103.

[29] L. Covi, H. B. Kim, J. E. Kim and L. Roszkowski, JHEP **0105** (2001) 033 [hep-ph/0101009].

[30] L. Covi, L. Roszkowski, R. Ruiz de Austri and M. Small, JHEP **0406** (2004) 003 [hep-ph/0402240].

[31] G. F. Giudice and A. Masiero, Phys. Lett. B **206** (1988) 480.

[32] P. Svrcek and E. Witten, JHEP **0606** (2006) 051 [hep-th/0605206].

[33] A. Arvanitaki, S. Dimopoulos, S. Dubovsky, N. Kaloper and J. March-Russell, Phys. Rev. D **81** (2010) 123530 [arXiv:0905.4720].

[34] A. Ringwald, Phys. Dark Univ. **1** (2012) 116 [arXiv:1210.5081 [hep-ph]].

[35] P. Arias, D. Cadamuro, M. Goodsell, J. Jaeckel, J. Redondo and A. Ringwald, JCAP **1206** (2012) 013 [arXiv:1201.5902 [hep-ph]].

[36] S. V. Troitsky, arXiv:1612.01864 [astro-ph.HE].

[37] J. Jaeckel and A. Ringwald, Ann. Rev. Nucl. Part. Sci. **60** (2010) 405 [arXiv:1002.0329 [hep-ph]].

[38] K. Baker *et al.*, Annalen Phys. **525** (2013) A93 [arXiv:1306.2841 [hep-ph]].

[39] M. Giannotti, I. Irastorza, J. Redondo and A. Ringwald, JCAP **1605** (2016) no.05, 057 [arXiv:1512.08108 [astro-ph.HE]].

[40] R. Daido, F. Takahashi and W. Yin, arXiv:1702.03284.

[41] A. Ringwald and K. Saikawa, Phys. Rev. D **93**, 085031 (2016); Addendum *ibid.* **94**, 049908 (2016) [arXiv:1512.06436].

[42] L. Fleury and G. D. Moore, JCAP **1601** (2016) 004 [arXiv:1509.00026].

[43] L. M. Fleury and G. D. Moore, JCAP **1605** (2016) 005 [arXiv:1602.04818].

[44] G. D. Moore, arXiv:1604.02356.

[45] P. Sikivie, Phys. Rev. Lett **51**(1983)1415; Erratum *ibid.* **51**(1983)695

[46] W. Chung, Launching axion experiment at CAPP/IBS in Korea, in *Proceedings of the 12th Patras Workshop on Axions, WIMPs and WISPs, Jeju, Korea* (2016), in preparation.

[47] D. Budker, P. W. Graham, M. Ledbetter, S. Rajendran and A. Sushkov, Phys. Rev. X **4**, (2014) 021030 [arXiv:1306.6089].

[48] P. Sikivie, N. Sullivan and D. B. Tanner, Phys. Rev. Lett. **112**, (2014) 131301 [arXiv:1310.8545].

[49] Y. Kahn, B. R. Safdi and J. Thaler, Phys. Rev. Lett. **117**, (2016) 141801 [arXiv:1602.01086].

[50] A. Arvanitaki and A. A. Geraci, Phys. Rev. Lett. **113**, (2014) 161801 [arXiv:1403.1290].

[51] A. Millar et al., JCAP **1701** (2017) no.01, 061, [arXiv:1612.07057]

[52] P. Arias et al, JCAP **06**(2012)013

[53] B. Döbrich et al., arXiv:[1410.0200v1]

[54] B. Majorovits and J. Redondo for the MADMAX working group, Contributed to the 12th Patras Workshop on Axions, WIMPs and WISPs, Jeju Island, South Korea, June 20 to 26, 2016, DESY-PROC-2016-03, [arXiv:1611.04549]

[55] S. Caspi et al., IEEE Transactions on Applied Superconductivity **24**(3)(2014) 4001804

[56] E. Rochepault, P. Vedrine and F. Bouillault. IEEE Transactions on Applied Superconductivity **22**(3)(2012)4900804

[57] X. Aupi et al., J. Appl. Phys **95**(5)(2004)2639

[58] T.Shimada et al., IEEE Transactions on Ultrasonics, Ferroelectrics, and Frequency Control, **57**(10)2010

[59] Journal of Nanomaterials, Volume 2014, Article ID 124814, http://dxdoi.org/10.1155/2014/124814

[60] T. Oxley, IEEE Trans. Microwave Theo. and Techn., **50**(3)(2002)867

[61] T. Mimura, IEEE Trans. Microwave theory and techn. **50**(3)(2002)780

[62] T. Hunter and R. Kimberk, [arXiv:1507.04280]

[63] A. Ringwald, L. Rosenberg and G. Rybka, Chin.Phys. C **38**(9)(2014)626

[64] E. Armengaud et al., JINST **9**(2014)T05002

[65] J. Suzuki, Y. Inoue, Tomoki Horie, M. Minowa, Proceedings contribution to the 11th Patras Workshop on Axions, WIMPs and WISPs, Zaragoza, June 22 to 26, 2015, [arXiv:1509.00785]